Journal of Chromatography A, 1228 (2012) 51–56

Contents lists available at ScienceDirect

Journal of Chromatography A

journal homepage: www.elsevier.com/locate/chroma

Development of a pressure-driven injection system for precisely time controlled attoliter sample injection into extended nanochannels

Ryo Ishibashi [a], Kazuma Mawatari [a,b], Katsuyoshi Takahashi [b], Takehiko Kitamori [a,b,*]

[a] Department of Applied Chemistry, School of Engineering, The University of Tokyo, 7-3-1 Hongo, Bunkyo, Tokyo 113-8656, Japan
[b] Department of Bioengineering, School of Engineering, The University of Tokyo, 7-3-1 Hongo, Bunkyo, Tokyo 113-8656, Japan

ARTICLE INFO

Article history:
Available online 6 June 2011

Keywords:
Nanofluidics
Sample injection
Extended-nanospace
Normal phase
Chip- based separation

ABSTRACT

The rapidly developing interest in nanofluidics, which is used to examine liquids on an order that ranges from an attoliter to a femtoliter, correlates with the recent interest in decreased sample amounts, such as in the field of single-cell analysis. For general nanofluidic analysis, the fact that a pressure-driven flow does not limit the choice of solvents (aqueous or organic) is an important aspect. In this paper, an automated injection system using a pressure-driven flow for several hundred nanometer-sized channels (extended nanochannels) is described. By automatically, and independently, switching four pressure lines using solenoid valves controlled by a sequencer with a time resolution of 10 ms, 550 aL sample band in minimum was reproducibly injected under normal phase conditions. The reproducibility of the band injection was improved by one order when compared with the previous injection method, which enables determination of time zero for injection. These facts are essential for the further band analysis in nanochannels, where diffusion is dominant. This injection system using pressure-driven flow can be used with any kind of solvent, which should make it a significant tool for nanofluidic applications, such as immunoassay, DNA analysis, and chromatography.

1. Introduction

The 10^1 to 10^3 nm scale space (so-called extended nanospace) has recently gained much attention, since it is transient space between single molecules and normal liquid and unique liquid properties are expected [1,2]. For example, water properties in an extended nanospace are reportedly altered, displaying higher viscosity, lower dielectric constant, and higher proton mobility [3–5]. Moreover, since the volume of liquid in a 10^1–10^3 nm scale space is on an attoliter level, the extended nanospace would be appropriate for the analysis of an extremely low-volume sample, such as in the field of single cell analysis. As the single cell trapping, lysis, and analysis is becoming to be integrated into a single microfluidic chip [6], further techniques for analysis of extremely low-volume sample should also be developed. A pressure-driven fluid control system using an air compressor and a pressure controller has been developed for the nanofluidic control [7]. Here, both ends of the extended nanochannels are connected to microchannels, which enable fast and secure liquid exchange. This alignment is essential for nanofluidic applications where complicated liquid handling is required. Some applications, such as conductivity measurement, immunoassay, and DNA analysis are performed using an extended nanospace [8–10].

Chromatography is an important application of extended nanofluidics, which has a potential of new separation mode due to the unique properties of extended nanospace. Here, the injection of an ultra-small volume of a sample band into an extended nanochannel is one of the main challenges for an effective separation. For a sample band injection into an extended nanochannel, electrokinetic pinched injection is the simplest method [11]. However, it is difficult to adapt an electrokinetic-driven flow to normal phase chromatography where non-polar organic solvents are used for the mobile phase. For reversed-phase separation, shear-driven chromatography was developed in a channel less than 1 μm deep [12]. The automated injection system resulted in a high reproducible band injection in a picoliter range [13]. Here, the top of the separation channel was hydrophobically modified in order to avoid a leakage of solution between the unbonded top and the bottom plates. In order to perform general chromatography in all chromatographic modes, pressure-driven chromatography shows the most promise.

Recently, we developed liquid chromatography using a pressure-driven flow in open column extended nanochannels (nanochromatography), which displayed the possibility for a highly

* Corresponding author at: Department of Applied Chemistry, School of Engineering, The University of Tokyo, 7-3-1 Hongo, Bunkyo, Tokyo 113-8656, Japan.
Fax: +81 3 5841 6039.
E-mail address: kitamori@icl.t.u-tokyo.ac.jp (T. Kitamori).

0021-9673/$ – see front matter © 2011 Elsevier B.V. All rights reserved.
doi:10.1016/j.chroma.2011.05.095

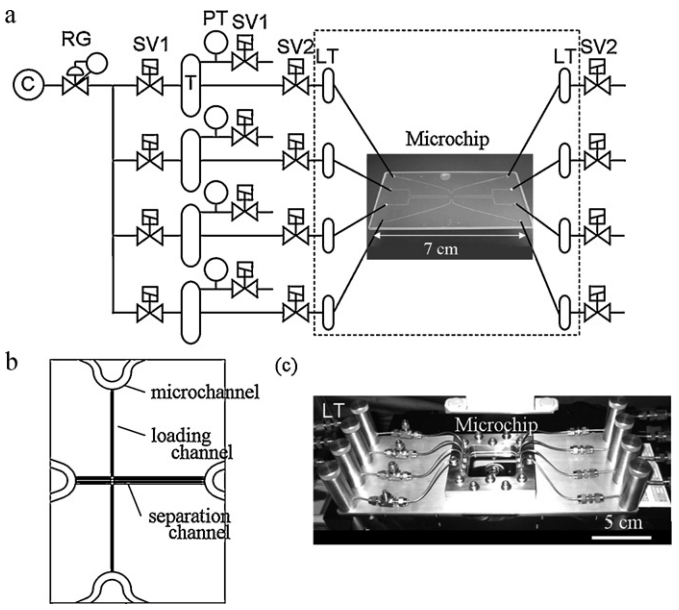

Fig. 1. Photograph of microchip and systematic chart of pressure-driven fluid control system (a). The abbreviations are defined as follows: compressor (C), regulator (RG), solenoid valve (SV), pressure transmitter (PT), air tank (T), and liquid tank (LT). Close-up of the extended nanochannel design (b). Nanochannels were 910 nm wide, 220 nm deep, and 1600 μm or 800 μm long from the cross-point, and the ends were connected to microchannels. Microchannels were 300 μm wide and 3 μm deep. Photograph (b) shows the custom-made chip holder (dashed line region in (a)).

efficient separation, by eliminating the factor of eddy diffusion due to the absence of packed columns [14]. Here, sample band was injected by manually switching pressures using three-way valves. However, control of this manual injection had a time resolution of 1 s, and a reliable chromatographic analysis of the band peak was difficult to obtain.

In this paper, we describe the development of a precise time-controlled injection system using the basics of our pressure-driven fluidic control technique in extended nanochannels. By controlling the switching of injection pressure in a time resolution of 10 ms, a sample band of 550 aL in minimum was successfully injected under normal phase conditions, with one-order improvement in reproducibility compared with our previous injection system. Precise control of the band injection enabled further analysis of the band in extended nanochannels.

2. Experimental

2.1. Chip fabrication and design

The extended nanochannels were fabricated on a quartz glass plate by electron beam lithography and plasma etching (photograph in Fig. 1a) [15]. The substrate with channels was thermally bonded with a cover plate in a vacuum furnace at 1080 °C. Dust and impurities were excluded during fabrication by performing all operations in class 100 and 1000 clean rooms. The design of the nanochannel consisted of a loading channel and three parallel separation channels, as shown in Fig. 1b. Each ends of the cross-shaped nanochannels (910 nm wide, 220 nm deep, 1600 or 800 μm long from the cross-point) were linked to microchannels (300 μm wide, 3 μm deep). Each end of the microchannels was connected to the exterior via through-holes.

2.2. Fluid control system and sample injection method

The systematic chart of the custom-made pressure-driven fluid control system is shown in Fig. 1a. Pressure was generated by a high-pressure air compressor (C) (EC 1445H, Hitachi Koki, Tokyo, Japan), which could generate a maximum pressure of 4.4 MPa. The airline was then separated into four individual lines, and connected to air tanks (T) with the capability to store pressure of a given value through control of a solenoid valve (SV1) (J262G001AC100, ASCO Japan Co., Ltd., Nishinomiya, Japan) with a pressure transmitter (PT). The airline was then connected to a liquid tank (LT) via a solenoid valve (SV2) (SV30A32P4P33E, Circle Seal, CA, USA). Opening and closing of this valve was controlled by a sequencer (MS2-H100, Keyence, Osaka, Japan) to a desired time resolution of 10 ms. When the valve was opened, the liquid inside the tank was pressurized into the microchip at a predetermined setup pressure. When the valve was closed, the liquid tank was exposed to atmospheric pressure. Tubes connecting the solenoid valves (SV2) and

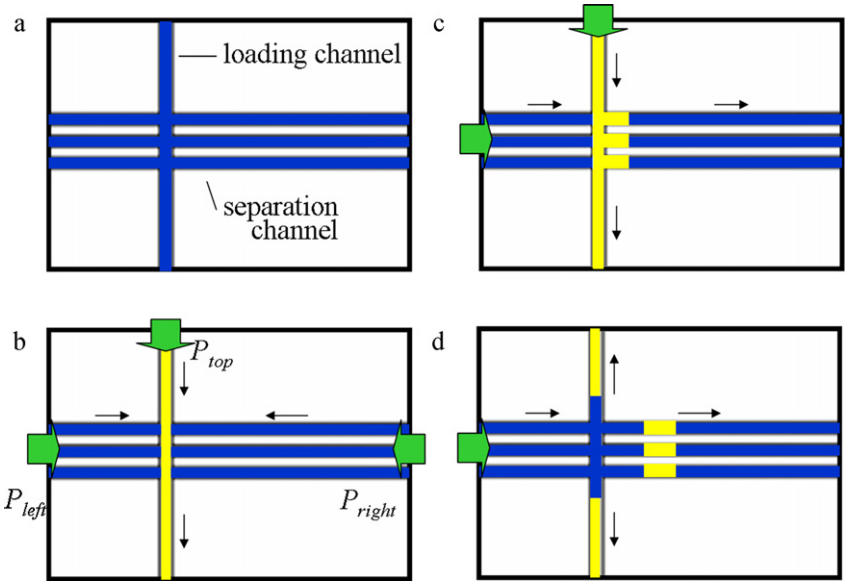

Fig. 2. Schematic view of pinched injection. In the initial state (a), channels are filled with a mobile phase. Pressure is applied from three ways for sample loading (b). For injection, first, P_{right} is switched off to atmospheric pressure (c). With a time lag, P_{top} is switched off for completion of injection (d). The small arrows indicate the direction of liquid flow.

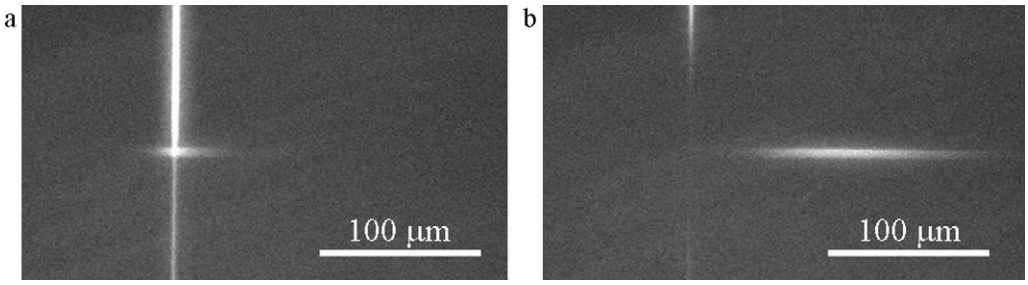

Fig. 3. Typical results of sample loading (a) and sample injection (b) under the following conditions: P_{top} = 320 kPa, P_{right} = 310 kPa, P_{left} = 300 kPa, and time lag of 0.2 s. The scale bar represents 100 μm.

liquid tanks could change position freely if necessary. The lines from the microchip were again connected to solenoid valves via liquid tanks, which were used as waste tanks. These solenoid valves also could sequentially control opening and closing. When these valves were opened, the liquid tank was exposed to atmospheric pressure. When the valve was closed, it worked as a stop valve. Fig. 1c shows a photograph of the liquid tank and microchip, including a custom-made chip holder. All the system including the chip holder was fabricated by Ohte Giken, INC. (Tsukuba, Japan). All parts of the holder were made of stainless steel, and all connections were made either by screwing or by silver brazing.

Pressure-driven pinched injection, which was first performed in a microchannel [16], was adapted to extended nanochannels, as shown in Fig. 2. Thick arrows indicate the presence of pressure, and line arrows show the direction of the liquid flow inside the nanochannels in the figure. First, both loading and separation channels were filled with a mobile phase (Fig. 2a). For sample loading, three pressures (P_{top}, P_{right}, P_{left}) were applied from the top of the loading channel, and from both ends of the separation channel (Fig. 2b). Then, P_{right} was switched off to atmospheric pressure to start introducing the sample into the separation channel (Fig. 2c). With a time lag (t_{lag}), P_{top} was switched off to cut off the sample band, and the band injection was completed (Fig. 2d). The timing of the switching-off of the pressures was controlled by a sequence with a time resolution of 10 ms. The concept of controlling fluid using solenoid valve was recently demonstrated in microchannels, using relatively small pressure (<200 kPa) [17]. We have evolved this concept as band injection device for nanofluidics.

2.3. Band observation

The microchip, including the custom-made chip holder (Fig. 1c) was placed on the motorized stage (BIOS 105T, Sigma Kouki Co., Ltd., Tokyo, Japan) of a fluorescence microscope, model IX71 (Olympus, Tokyo, Japan). A CCD camera (ImagEM, Hamamatsu, Shizuoka, Japan) was used to detect the fluorescence image, and software (Aquacosmos, Hamamatsu) was used for the analysis. In order to achieve the chromatogram, a time profile of the average intensity was obtained in a detection window at an arbitrary place in the recorded image. Pyrromethene 597 (EXCITO INC., Dayton, USA) was used as a fluorescence dye (50 μM), and a mixture of toluene/ethanol = 100/1 (v/v) was used as the mobile phase.

3. Results and discussions

3.1. Sample injection – proof of principle

The sample was chosen to show the injection availability under normal phase conditions, which could be achieved only by a pressure-driven flow. The mobile phase was toluene (non-polar solvent) and the stationary phase was the channel wall, which was bare silica (silanol surface, polar). Toluene is an aprotic solvent with very low dielectric constant (ε = 2.4), in which condition that the solute ions will not dissociate, and tend to keep neutral species [18,19]. The electrokinetic effect due to the electrical double layer in the several hundred nm channel will therefore not be discussed in this report.

Fig. 3 shows the typical results of a sample injection when P_{top} = 320 kPa, P_{right} = 310 kPa, P_{left} = 300 kPa, and time lag (t_{lag}) = 0.2 s. The three separation channels appeared as a single channel in this scale. The programmed sequence allowed 12 s of sample loading (Fig. 3a), and a sample injection was accomplished in one serial run (Fig. 3b).

Fig. 4 shows the band formation profile under the same conditions as depicted in Fig. 3 (P_{left} = 300 kPa, t_{lag} = 0.2 s). The longitudinal axis in the graph represents the average intensity through the separation channel. The time interval between the curves was 0.1 s. Curve (1) shows the sample loading state where the sample bandwidth kept constant by the mass equilibrium of diffusion and the flow toward the injection point. Curve (2) depicts the moment directly after the P_{right} was switched off, and curve (3) depicts the moment after P_{top} was switched off. The right-hand shoulder of the band increased during curves (2) and (3), due to the analytes entering the separation channel, as explained in Fig. 2c. When P_{right} was switched off, the sample band injection was completed in about 0.2 s, which agrees well with the value of t_{lag} Sample band kept broadening after injection (after curve (3)), keeping the symmetric gaussian profile.

Fig. 5 shows the dependence of t_{lag} and the injection band. The chromatograms were taken at 50 μm from the injection point. When t_{lag} was small (or zero), the sample entering the separation channel was insufficient and was diluted, which resulted in a lack of detection sensitivity. Conversely, when t_{lag} was large, the bandwidth and intensity increased. As in chromatography where

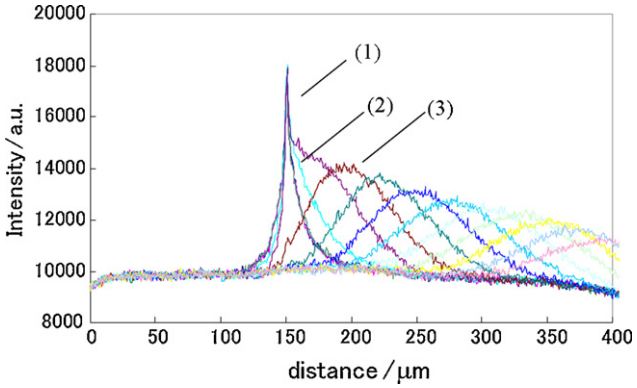

Fig. 4. Formation of the band after injection. Time interval between the curves is 0.1 s. Curve (1) represents sample loading, curve (2) shows conditions just after P_{right} was switched off, and curve (3) shows conditions just after P_{top} was switched off.

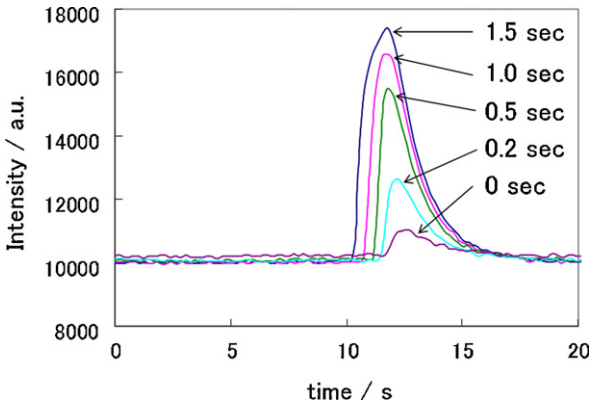

Fig. 5. Chromatogram of injected band when the time lag (t_{lag}) was varied. Sensitivity and bandwidth reduced with a decreasing time lag, and vice versa.

a smaller injection bandwidth is desired for higher separation efficiency, t_{lag} is a trade-off between detection sensitivity and bandwidth. Because the peak of the injection band is largely influenced by the t_{lag}, even on the order of 0.1 s, precise control of t_{lag} is necessary for reproducible injection.

Fig. 6 compares the repeatability of the five automated and manual sample injection runs using the same chip, P_{left} (= 300 kPa), and sample (pyrromethene 597 in toluene). Both the relative standard deviation of the peak maximum and the peak area were improved one order, from 42 to 3.5% and from 46 to 4.0%, respectively. The maximum difference of the peak arrival time between different runs improved from around 1 s to 0.1 s. This improvement is important for analysis of bandwidth in nanochannels, where the band broadening by diffusion will largely contribute to the bandwidth, even in the small time scale (*e.g.*, 190 μm for 1 s, and 60 μm for 0.1 s). High reproducible injection leads to determination of time zero for injection. When collecting data in nanochromatography, the camera is focused downstream from the separation channel, so the injection cannot be observed. Therefore, the precise peak arrival time after injection of the injected band cannot be measured with lack of highly reproducible injection. The two factors, high reproducibility and determination of the time zero after the injection, enables further band analysis of the chromatogram in nanochannels. Band shape was asymmetric in Fig. 6a, but symmetric in Fig. 6b. The asymmetric shape is not due to tailing by the adsorption of the analyte to the channel, as the band has a symmetric, gaussian profile in Fig. 4. Thus the asymmetric shape in Fig. 6a is probably observing the formation state of the gaussian band (between curves 1 and 3 in Fig. 4). Fig. 6b is not observing the formation state of the gaussian state due to the rise time of pressure is very slow (about 5 s) in the previous set-up, compared to present device (<1 s).

3.2. Band broadening

Band broadening was observed between sample loading and injection (from 57 to 130 μm, in full width) as can be seen in Fig. 3 or Fig. 4 curves (1) to (3). This band broadening is not favorable for chromatography, where the separation efficiency or the theoretical plate height is related to the injection bandwidth, and the increase of band width will decrease the separation efficiency. In order to understand this band broadening, bandwidth (full width at half maximum, $w_{0.5}$) was plotted against time. Fig. 7a shows the dependence of square bandwidth ($w^2{}_{0.5}$) against time, when the applied pressure was fixed to a constant value (P_{left} = 300 kPa), and t_{lag} was varied between 0 and 1.0 s. The dashed line in the figure indicates the boundary of (i) sample loading state, (ii) injection state, and (iii) after injection, and the figures on the top shows the direction of pressure in each state. The dashed line at the left is bent to show the point where the injection state was started with different t_{lag}. In the loading state (i), the bandwidth kept a constant value by the mass equilibrium of diffusion and the flow toward the injection point, as described in Fig. 4, curve (1). In the injection state (ii), the bandwidth largely increased during the t_{lag}. The slope of broadening corresponded to t_{lag}, where the increase was minimum ($w_{0.5}$ = 10–23 μm) when t_{lag} = 0 s, and maximum ($w_{0.5}$ = 10–170 μm) when t_{lag} = 1.0 s. This band broadening is due to diffusion during t_{lag}, and the flow toward the injection channel during the t_{lag} as depicted in Fig. 2c. The band broadening due to diffusion (full width, w_{diff}) can be expressed by the Einstein equation of diffusion as;

$$w_{diff} = 4\sigma = \sqrt{32 \times D_{mol} \times t_{\mathrm{det}}} \quad (1)$$

where D_{mol} is the molecular diffusion coefficient of the analyte. The bandwidth ($w_{0.5}$) at the end of injection state had a linear relation with t_{lag}. As can be seen in the plot of t_{lag} = 1.0 s, the rise time of band broadening did not respond with the beginning of t_{lag}, due to the analysis was on full width at half maximum. The point below the half maximum responded to the beginning of t_{lag}, but did not appeal in the plot. After injection (iii), the bandwidth kept on broadening gradually, where $w^2{}_{0.5}$ increased linearly with time. This broadening is consistent with diffusion and Taylor dispersion in the separation channel. Plots of t_{lag} = 0 s had a relatively large variance due to the small signal-to-noise ratio, as discussed in Fig. 5. Fig. 7b shows the dependence of square bandwidth ($w^2{}_{0.5}$) to time, when t_{lag} was fixed to a constant value (0.5 s), and applied pressure (P_{left}) was varied between 300 and 1000 kPa. The number of plots at 1000 kPa is small, due to the fast protrusion of the band from the detection window in this high pressure condition. Loading state (i) and after injection (iii) showed a similar behavior as discussed in Fig. 7a. In the injection state (ii), the slope of broadening this time corresponded to applied pressure, where the increase was minimum ($w_{0.5}$ = 9–96 μm) when 300 kPa, and

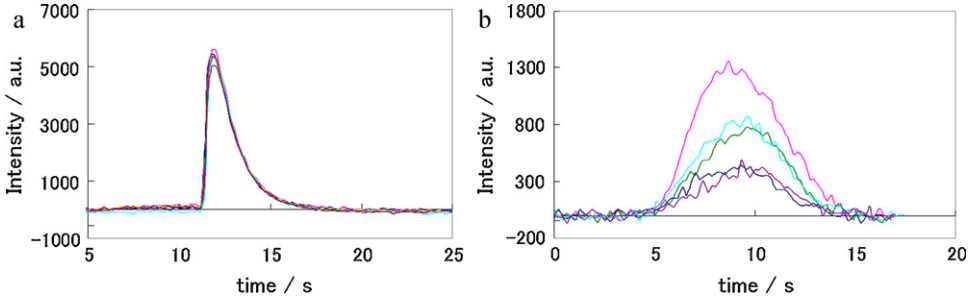

Fig. 6. Comparison of reproducibility of automated (a) and manual (b) sample injections. Chromatograms of five independent injections were taken at 50 μm from the injection points. The relative standard deviation of peak height was reduced from 42 to 3.5%, and that of the peak area was reduced from 46 to 4.0% by automating the injection.

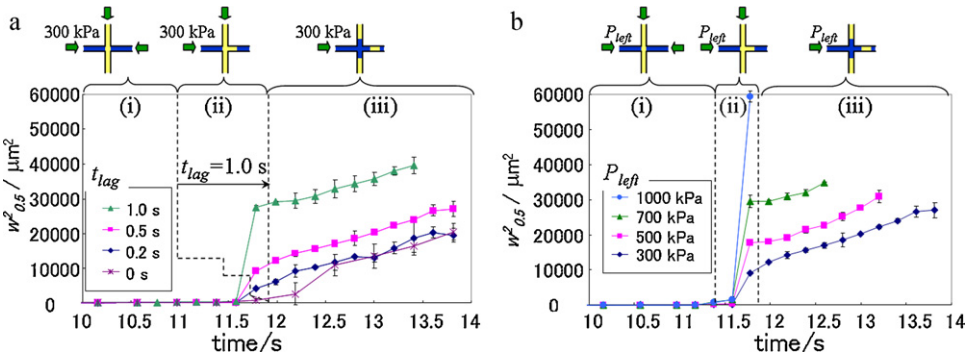

Fig. 7. Dependence of square bandwidth ($w^2_{0.5}$) against time, when the applied pressure was fixed to a constant value (P_{left} = 300 kPa), while t_{lag} was varied (a), and when t_{lag} was fixed to a constant value (0.5 s), while applied pressure (P_{left}) was varied (b). The dashed line in the figure indicates the boundary of (i) sample loading state, (ii) injection state, and (iii) after injection, and the figures on the top shows the direction of pressure in each state.

maximum ($w_{0.5}$ = 6–244 μm) when 1000 kPa. This band broadening is again due to the diffusion and the flow toward the injection channel during the t_{lag}. The bandwidth ($w_{0.5}$) at the end of injection state had a linear relation with applied pressure. As the bandwidth after injection state had a linear relation with both applied pressure (*i.e.,* flow velocity originated by this pressure) and t_{lag}, this band broadening (full width, w_{flow}) can be expressed as a product of flow velocity (v) and t_{lag}, as

$$w_{flow} = v \times t_{lag} \quad (2)$$

which indicates that the flow during t_{lag} is dominant to this band broadening in injection state.

As a result, the band broadening in injection is consisted by; 1. Bandwidth in loading state (w_{load}), 2. Diffusion during injection, and 3. Flow toward the injection channel during injection. Thus the calculated injection bandwidth (full width, $w_{inj,calc}$), using Eqs. (1) and (2), can be expressed as

$$w_{inj,calc} = \sqrt{w^2_{load} + w^2_{flow} + w^2_{diff}} \quad (3)$$

The first factor of bandwidth can be controlled by the pressure balance during the sample loading state, though it is not much a problem while its contribution is small. The second factor, broadening due to diffusion, can be reduced by reducing t_{lag}. However, the reduction of t_{lag} leads to a reduction in sensitivity, so it cannot be wiped out completely in many cases. Third factor, flow during the injection was the most dominant factor in band broadening. As this factor could be expressed by the product of flow velocity and t_{lag}, it can be controlled by controlling the applied pressure and t_{lag}. Our present device enables to control the t_{lag} with the time resolution of 10 ms, thus led to a reproducible injection.

The volume of the injected sample corresponds to the sum of the volume of the intersection of loading and separation channels (0.91 μm × 0.91 μm × 0.22 μm × 3 channels = 550 aL), and sample pushed into the separation channel by the flow during the t_{lag} (w_{flow} × channel depth). The flow velocity was calculated by measuring the fluorescence signal between several points in the separation channel, by serial experiments. The calculated injection volume when t_{lag} = 0.2 s and P_{left} = 300 kPa, was 4.9 fL (36 μm s^{-1} × 0.2 s × 0.91 μm × 0.22 μm × 3 channels + 550 aL, 1.6 fL for single separation channel), and 550 aL (180 aL for single separation channel) in minimum, when t_{lag} = 0 s. This amount was three to four orders smaller than that used by Desmet's group, who also automated the injection of an extended-nanochannel by a pL order, but with a shear-driven flow [12]. For the analysis of an ultra-small volume of sample, *e.g.*, in the field of single-cell proteomics where the volume of a single cell is on the order of pL, the handling of the aL to fL range for analysis should be suitable.

4. Conclusions

We have developed an automated injection system using pressure-driven flow in extended nanochannels by controlling the four pressure lines, and by switching the pressures ON and OFF using sequence-controlled solenoid valves. By precisely controlling the time lag with a time resolution of 10 ms, a sample injection of 550 aL in minimum was achieved, which is four orders smaller than a conventional injection device. The reproducibility of the injected band peak was improved by one order compared to our previous method. High reproducibility of the band and determination of time zero after the injection were achieved, which enabled further analysis of the band. Band broadening was observed between loading and injection, and was discussed as the combination of bandwidth upon sample loading, sample flow during switching pressure, and diffusion. As we have performed the injection under normal phase condition, pressure-driven flow does not limit the choice of solvents. This device enables cutting of definite volume sample of aL to fL in extended nanospace Therefore, it would be a powerful tool for applications in nanofluidic systems, such as immunoassay [8], DNA analysis [10], and chromatography. Basic analysis of physicochemical properties in extended nanospace can also be achieved, such as diffusion coefficient measurement by band cutting. Normal phase separation using this device is now being performed.

Acknowledgement

This work was supported by Grant-in-Aid for Specially Promoted Research from the Japan Society for the Promotion of Science (JSPS), and JSPS KAKENHI (21-7507).

References

[1] A. Hibara, T. Tsuahara, T. Kitamori, J. Chromatogr. A 1216 (2009) 673.
[2] M.L. Kovarik, S.C. Jacobson, Anal. Chem. 81 (2009) 7133.
[3] A. Hibara, T. Saito, H.-B. Kim, M. Tokeshi, T. Ooi, M. Nakao, T. Kitamori, Anal. Chem. 74 (2002) 6170.
[4] T. Tsukahara, A. Hibara, Y. Ikeda, T. Kitamori, Angew. Chem. Int. Ed. 46 (2007) 1180.
[5] N.R. Tas, J. Haneveld, H.V. Jansen, M. Elwenspoek, A. Van den Berg, Appl. Phys. Lett. 85 (2004) 3274.
[6] B. Huang, H. Wu, D. Bhaya, A. Grossmann, S. Granier, B.K. Kobilka, R.N. Zare, Science 315 (2007) 81.
[7] T. Tsukahara, K. Mawatari, A. Hibara, T. Kitamori, Anal. Bionanal. Chem. 391 (2008) 2745.
[8] R. Kojima, K. Mawatari, B. Renberg, T. Tsukahara, T. Kitamori, Microchim. Acta 164 (2009) 307.
[9] K. Morikawa, K. Mawatari, M. Kato, T. Tsukahara, T. Kitamori, Lab Chip 10 (2010) 871.
[10] H. Xi, B. Renberg, K. Sato, K. Mawatari, M. Nilsson, T. Kitamori, Proceedings of the 13th International Conference on Miniaturized Systems for Chemistry and Life Sciences, 2009, p. 1554.

[11] S. Pannathur, J.G. Santiago, Anal. Chem. 77 (2005) 6782.
[12] D. Clicq, N. Vervoort, R. Vounckx, H. Ottavaere, J. Bujis, C. Gooijer, F. Ariese, G.V. Baron, G. Desmet, J. Chromatogr. A 979 (2002) 33.
[13] W.D. Malsche, D. Clicq, H. Eghbali, V. Fekete, H. Gardeniers, G. Desmet, Lab Chip 6 (2006) 1322.
[14] M. Kato, M. Inaba, T. Tsukahara, K. Mawatari, A. Hibara, T. Kitamori, Anal. Chem. 82 (2010) 543.
[15] T. Tsukahara, T. Kuwahata, A. Hibara, H.-B. Kim, K. Mawatari, T. Kitamori, Electrophoresis 30 (2009) 3212.
[16] X. Bai, H.J. Lee, J.S. Rossier, F. Reymond, H. Schafer, M. Wossner, H. Girault, Lab Chip 2 (2002) 45.
[17] P.B. Allen, G. Milne, B.R. Deopker, D.T. Chiu, Lab Chip 10 (2010) 727.
[18] A. Karbaum, T. Jira, Electrophoresis 20 (1999) 3396.
[19] M.-L. Riekkola, Electrophoresis 23 (2002) 3865.